# Solution NMR Study of the Structural Basis of the Bohr Effect in the Monomeric Hemoglobins from *Chironomus thummi thummi*†

Wei Zhang,‡ Klaus Gersonde,§ and Gerd N. La Mar*,‡

*Department of Chemistry, University of California, Davis, California 95616, and Fraunhofer-Institut für Biomedizinische Technik and Lehrstuhl für Medizintechnik, Universität des Saarlandes, D-66386 St. Ingbert, Germany*

*Received October 22, 1996; Revised Manuscript Received December 5, 1996*⊗

ABSTRACT: The larva of the midge *Chironomus thummi thummi* possesses two monomeric hemoglobins, HbIII and HbIV, with extensive sequence homology, which exhibit marked but differential Bohr effects (pH influence on ligand affinity). These Hbs serve as ideal models for allosteric control of ligand affinity via tertiary-only structural changes. The cyanomet derivatives of these two Hbs have been shown to possess essentially indistinguishable heme cavity structures in solution at low pH (Zhang et al., 1996) that are also very similar to that of the low pH form of HbIII in the crystal (Steigemann & Weber, 1979). 2D $^1$H NMR has been utilized to elucidate the solution heme cavity structure of the alkaline form of the cyanomet derivatives of HbIII and HbIV to identify the Bohr proton binding site and characterize the nature of the structural changes that accompany the allosteric transition. Significant structural changes with pH have been identified in two regions of the heme cavity, near the axial His and at the junction of pyrroles B and C. The Bohr proton site is identified as His94, which at low pH makes a salt bridge to the terminal Met136. The rupture of this salt bridge at high pH leads to the expulsion of the Met136 side chain next to the His F8 ring where it serves as a spacer between the heme and F-helix, and leads to a cascade of side chain reorientations in the densely packed hydrophobic interior involving five Phe (65, 66, 128, 129, 133), Val132, and Ile69, all on the E- and H-helices. The terminal member of the cascade, Phe65, which acts as a spacer between the E- and F-helices at low pH, is rotated toward the heme plane. The conversion of the low pH, low-affinity "tense" to the high pH, high-affinity "relaxed" state is primarily due to the removal of the Met136 and Phe65 spacers. A central residue in transmitting the Bohr effect from His94 to Phe65 is residue 132. In HbIV, Val132 provides a cavity in the hydrophobic core to readily accommodate the initial step in rotating the Phe129 side chain. In HbIII, the Ile132 provides tight packing to all neighboring side chains and hence would inhibit the rotation of the Phe129 side chain. It is proposed that the lone internal residue difference between HbIII (Ile132) and HbIV (Val132) is the primary basis for the different amplitudes of their Bohr effect.

The oxygen affinity of vertebrate hemoglobins, Hbs,[1] is controlled by a variety of allosteric effectors that include protons (Bohr effect), polyphosphates, carbon dioxide, and ligation state of nearby subunits (cooperativity) (Dickerson & Geis, 1983; Perutz et al., 1987). The allosteric effectors in these tetrameric Hbs effect both quaternary and tertiary structure in a complex manner that precludes simple separation of the various influences. The larva of the midge *Chironomus thummi thummi, CTT,* possesses at least twelve Hbs (Braunitzer & Braun, 1965), of which three are monomeric in all oxidation/ligation states and two of these, labeled HbIII and HbIV, exhibit marked but differential Bohr effects (Sick & Gersonde, 1969; Gersonde et al., 1972, 1976; Gersonde & Sick, 1974, Ruf et al., 1994). HbIII and HbIV share 85% sequence identity (Buse et al., 1979; Pfletschinger et al., 1980) and nineteen of the twenty conservative substitutions are for residues which extend to the protein surface (Steigemann & Weber, 1979). The one substitution for a buried residue is at position 132(H18) where the Ile in HbIII is substituted by Val in HbIV. Hence these monomeric HbIII and HbIV serve as the simplest models for elucidating the solely tertiary structural basis of the allosteric control of the ligand affinity due to the titration of a single remote residue (Bohr effect). The low-affinity **t** (for tense) and high-affinity **r** (for relaxed protein) states are most simply related by eq 1:

$$\mathbf{t} \rightleftarrows \mathbf{r} \qquad (1)$$

As the Bohr effect is a typical reciprocal effect, the position of the equilibrium is modulated by both the protonation state of the Bohr residue and the iron ligation state. There need not be a one-to-one correspondence between the protonation state and the affinity state. The deprotonation of the deoxy state already results in a transition from a tense (deoxy) into a relaxed (deoxy) state. On the other hand, the ligated (oxy) form can exist in the Bohr protonated and non-protonated state [see Figure 7 in Gersonde et al, (1986a)]. Solution $^1$H NMR studies of the His ring chemical shifts of both HbIII

† This research was supported by grants from the National Institutes of Health, HL 16087 (G.N.L.), the Fonds der Chemischen Industrie (K.G.), and the Deutsche Forschungsgemeinschaft (K.G.).

* Corresponding author. Phone: (916) 752-0958. FAX: (916) 752-8995. E-mail: lamar@indigo.ucdavis.edu.

‡ University of California, Davis.

§ Universität des Saarlandes.

⊗ Abstract published in *Advance ACS Abstracts,* February 1, 1997.

[1] Abbreviations: *CTT, Chironomus thummi thummi*; Hb, hemoglobin; Mb, myoglobin; NOE, nuclear Overhauser effect; NOESY, 2D nuclear Overhauser spectroscopy; TOCSY, 2D total correlation spectroscopy; COSY, 2D correlation spectroscopy; DSS, 2,2′-dimethyl-2-silapentane-5-sulfonate.

S0006-2960(96)02646-3 CCC: $14.00 

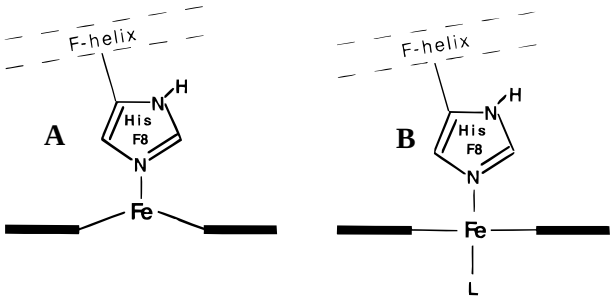


FIGURE 1: Schematic representation of the (A) deoxy or unligated Hb structure with the iron, well out of the heme plane on the side of the proximal His(F8), and (B) ligated Hb with the iron in-plane with the heme. The conversion of unligated to ligated heme results in a decrease in the distance between the heme plane and the F-helix.

and HbIV have demonstrated that the Bohr proton originates from either His94(G2) or His111(G19). The p*K* of one of these two His was found to be sensitive to the oxidation/ligation state of the heme iron, confirming that the allosteric transition can be induced in all oxidation/ligation states (Sick et al., 1972; Sick & Gersonde, 1974; Steffens et al., 1977).

A common feature of all interpretations of the control of ligand affinity by tertiary structure involves the position of the proximal F-helix relative to the heme plane and the interactions with its neighbors in the protein (Perutz et al., 1987). The unligated or deoxy heme iron is five-coordinated and high-spin, with the iron 0.5−0.8 Å out of the heme plane; upon ligation, the iron converts to low-spin and the iron (pulling its axial His) moves into the heme plane, as shown in Figure 1. This movement slightly weakens the Fe−His bond, which, by the *trans* effect, strengthens the Fe−ligand bond and increases ligand affinity (Gersonde et al., 1986b) The modulation of the ligand affinity then involves interactions that impede the movement toward the heme of the F-helix with the axial His.

*Chironomus* HbIII provided one of the earliest high-resolution crystal structures for a variety of oxidation/ligation states in the low-affinity or **t** tertiary state at low pH (Huber et al., 1971; Steigemann & Weber, 1979; Hartmann et al., 1987). The protein exhibits the normal Mb fold but with the exceptional feature that the distal His E7, implicated in ligation control in vertebrate Hb, is not oriented into the heme cavity but out toward the solution in all but one state. In the crystal, the cyanomet form exhibits an orientation of His E7 which is disordered ∼1:1 with His E7 oriented into the pocket and interacting with the ligand, and turned out of the pocket (Steigemann & Weber, 1979). Inasmuch as the HbIII crystals could not withstand the structural perturbations of the Bohr deprotonation, there exists no information on the nature of the structural changes that accompany the transition in eq 1.

Solution $^1$H NMR studies of the molecular structure, and its sensitivity to pH, for the *Chironomus* Hbs have been severely hampered because of the presence of two distinct molecular heterogeneities (La Mar et al., 1978a,b, 1980; Krümpelmann et al., 1980; Ribbing & Rüterjans, 1980; Peyton et al., 1988). For both HbIII and HbIV, the heme exhibits significant orientational heterogeneity about the α,γ-*meso* axis, and for HbIII, there is a further silent mutation at Thr/Ile(E6) (Buse et al., 1979), resulting in severe spectral congestion. The spectral congestion in the paramagnetic ($S = {}^1/_2$) cyanomet Hb form is reduced, particularly near the

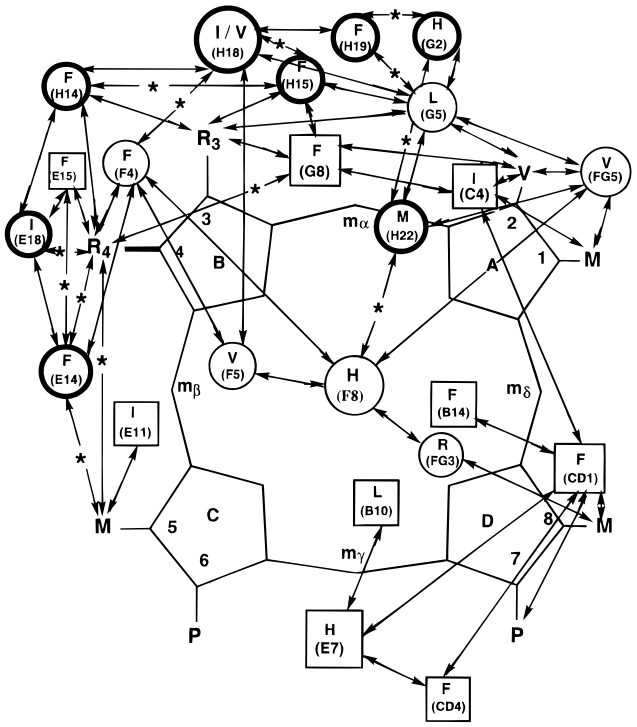


FIGURE 2: Schematic representation of the heme pocket structure of *CTT* Hbs and of the surrounding environment involved in the allosteric transition. Proximal and distal residues are represented by circles and squares, respectively. Observed dipolar contacts are represented by lines with double-sided arrows. Dipolar contacts which *change significantly* during the allosteric transition are shown by asterisks in the center of the double-sided arrow, and amino acid side chains or heme substituents whose orientations are concluded to be significantly perturbed by the allosteric transition are shown in bold.

heme cavity, because of the sizable hyperfine shifts induced by the high paramagnetic anisotropy of the iron (La Mar et al., 1978a,b, 1980; Peyton et al., 1988, 1991; Zhang et al., 1996). Earlier $^1$H NMR studies of both cyanomet HbIII and HbIV had shown that some hyperfine-shifted heme signals exhibited a strong pH effect that could be correlated with the titration of a His ring signal (La Mar et al., 1978a; Peyton et al., 1991). The large 4-vinyl shift changes were proposed to arise from altered oscillatory mobility/position at high and low pH (La Mar et al., 1978b). Recent $^1$H 2D NMR studies on the cyanomet HbIII and HbIV in acidic solution (**t** state) allowed the assignment of residues in the heme cavity by a combination of standard 2D methods as applied to paramagnetic systems (La Mar & de Ropp, 1996), and augmented by steady-state NOEs, paramagnetic relaxation, and quantitative interpretation of the dipolar shifts (Zhang et al., 1996). This study demonstrated that in solution, in contrast to the crystal (Steigemann & Weber, 1979), cyanomet HbIII has the distal His E7 exclusively turned into the pocket and interacting with the bound ligand (Zhang et al., 1996). Otherwise, the observed dipolar shifts in solution reflected a heme cavity that is essentially indistinguishable from that in the crystal with His E7 in the pocket. Finally, detailed comparison of cyanomet HbIII and HbIV revealed very similar solution structures in the heme cavity, which is consistent with the highly conserved sequence near the active site. The relevant residues and their dispositions relative to the heme and each other in cyanomet HbIV are shown schematically in Figure 2.

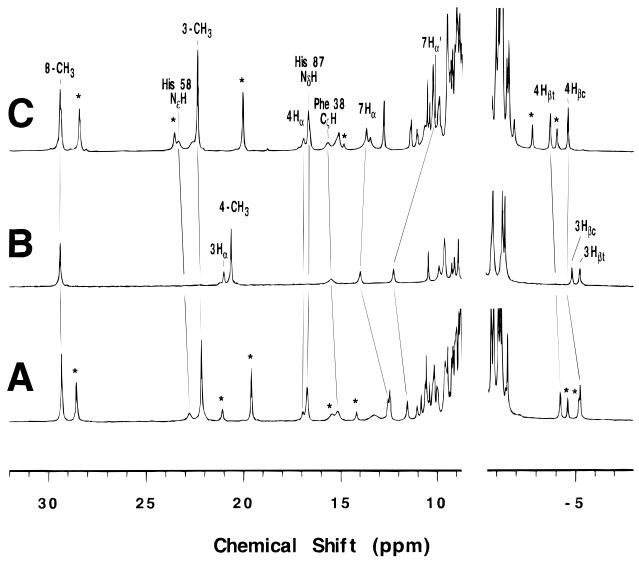


FIGURE 3: Resolved portions of the 500 MHz $^1$H NMR spectra at 20 °C and pH 8.5 for (A) *CTT* cyanomet HbIV in $^1H_2O$, (B) *CTT* cyanomet HbIV* (containing protohemin-III with 3-vinyl and 4-methyl) in Figure 2 in $^2H_2O$, and (C) *CTT* cyanomet HbIII in $^1H_2O$. For both native HbIII and HbIV, which exhibit heme orientational disorder, only the resonance assignments for the major rotational isomers are given; minor isomeric peaks are labeled with asterisks; the symmetric protoheme-III in HbIV* ($R_3$ = vinyl, $R_4$ = methyl in Figure 2) results in a homogeneous protein with a single set of peaks labeled so as to correspond to the numbering of the major isomer in cyanomet HbIII and HbIV.

In this report, we extend the solution NMR description of the two *Chironomus* cyanomet Hbs to alkaline pH. Our goals are to assign the Bohr proton site, identify the nature of structural changes that accompany the Bohr transition, and by comparison of cyanomet HbIII and HbIV with their differential Bohr effect amplitudes (Gersonde et al., 1972, 1986; Sick & Gersonde, 1974; Buse et al., 1979), deduce a plausible mechanism for the Bohr effect that would guide mutagenic approaches (Kao et al., 1994). Because of the more favorable heme orientational disorder in HbIV (~3:1) than HbIII (~3:2) (see Figure 3) and the absence of the silent mutation that plagues HbIII, our analysis will emphasize cyanomet HbIV, and sufficient data are presented to allow a comparison of the high-pH forms of the two Hbs.

## MATERIALS AND METHODS

*Protein.* Native HbIII and HbIV from *Chironomus thummi thummi* (*CTT*) possessing protohemin-IX ($R_3$ = methyl, $R_4$ = vinyl in Figure 2) were prepared as described previously (Gersonde et al., 1972; La Mar et al., 1983; Ruf et al., 1994). The cyanide complexes were prepared by adding ~10-fold excess of KCN to a ~2 mM metHb solution. The pH was adjusted with $NaO^1H$($NaO^2H$) or $^1$HCl($^2$HCl) in $^1H_2O$($^2H_2O$) solution, and measured with an Ingold microcombination electrode and a Beckman model 3550 pH meter. The structure analysis was performed at pH 8.5 where the Bohr proton site is only ~90% deprotonated. This value was selected because of the strong base catalysis for several key labile protons precluded assignments at higher pH. A ~1 mM solution of *CTT* HbIV reconstituted with the symmetric protohemin-III (4-methyl and 3-vinyl instead of 4-vinyl and 3-methyl in Figure 2) in $^2H_2O$, designated HbIV*, is the same sample described previously (La Mar et al., 1980; Zhang et al., 1996).

*NMR Data.* All $^1$H NMR data were collected on a GE Omega 500 spectrometer operating at 500 MHz. The observed chemical shifts, $\delta_{DSS}$(obs), are referenced to 2,2′-dimethyl-2-silapentane-5-sulfonate, DSS, via the solvent signal. Solvent suppression, when necessary, was achieved by direct saturation during the relaxation delay. Phase-sensitive TOCSY (Braunschweiler & Ernst, 1983; Bax & Davis, 1985), NOESY (States et al., 1982), and *n*-type COSY (Bax, 1981) were collected (512 $t_1$ blocks × 2048 $t_2$ points) in order to identify scalar and dipolar connectivities among heme and amino acid residues. Two different spectral widths and mixing times were used, 26−30 kHz and 40−50 ms mixing times to cover the complete spectrum, and 8.0−10 kHz and 110 ms mixing time to cover the diamagnetic region with better resolution. The 90° pulse width was ~8 $\mu$s (~25 $\mu$s for TOCSY). The repetition time was ~0.7 s per scan for 26−30 kHz and 1.2s for 8.0−10 kHz windows. 96−256 scans were collected for each block. 2D data sets were processed by FELIX software on a Silicon Graphics work station as described in detail previously (Qin & La Mar, 1992).

*Magnetic Axes Determination.* The magnetic axes for the alkaline form of cyanomet HbIV were determined in the identical manner as described in detail for the acidic form of the Hb (Zhang et al., 1996) and other cyanomet Mbs (Emerson & La Mar 1990; Rajarathnam et al., 1992, 1993; Qin et al., 1993). The resulting magnetic anisotropies and orientation of the magnetic axes are indistinguishable from the values reported for cyanomet HbIII and HbIV at acidic pH (Zhang et al., 1996; not shown; see Supporting Information).

## RESULTS

The assignment and structural analysis were carried out on the major heme orientational isomer of cyanomet HbIV in $^1H_2O$ (La Mar et al., 1980; Peyton et al., 1988; Zhang et al., 1996). Since spectral congestion in the diamagnetic envelope even for cyanomet HbIV precludes complete assignments and total structure determination, our studies will focus on residues that line the active site and/or residues which exhibit significant chemical shift or NOESY cross peak pattern changes with the allosteric transition. Hence, while the structural analysis will be incomplete, the results derived from our analysis provide insight into the mechanism of the Bohr effect. Our focus will be to first identify the residues which are "stationary" during the allosteric transition. This work will be followed by locating at least the key residues whose positions can be demonstrated to change in the allosteric transition. Initially, the altered orientations will be interpreted as representing the complete population of the **r** state. Subsequent evaluation of this assumption, together with the comparison to cyanomet HbIII, in fact, suggest that the **r** state is only fractionally populated even with complete deprotonation of the His Bohr proton (see Discussion). The resolved portions of the 500 MHz $^1$H spectra for cyanomet HbIV, HbIV*, and HbIII at pH 8.5 are shown in Figure 3A, 3B, and 3C, respectively. Since the assignments for the low-pH form of both Hbs have been reported, $^1$H NMR data are shown only to document *significant changes* in dipolar contacts near the heme in cyanomet HbIV. Upon identification of the structural changes with pH for cyanomet HbIV, sufficient assignments

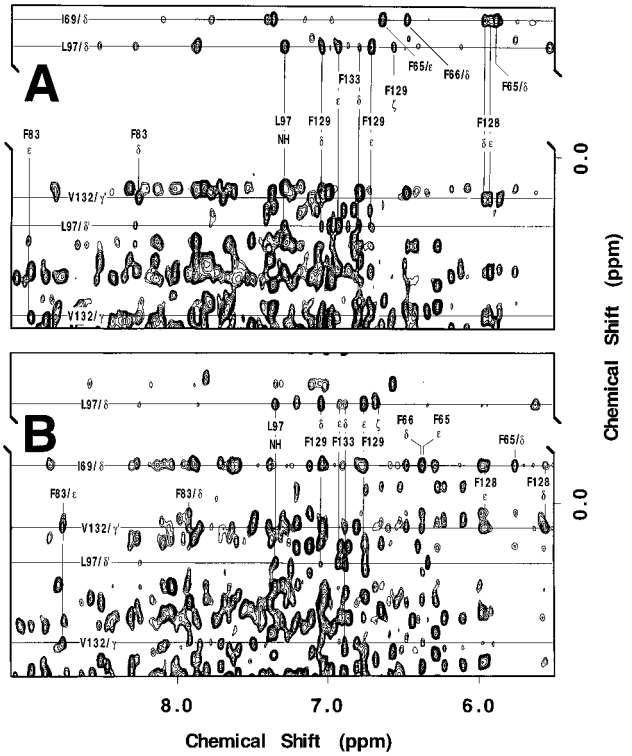


FIGURE 4: 500 MHz $^1$H NMR NOESY spectra ($\tau_m$ = 110 ms) for cyanomet HbIV in $^1H_2O$ at 20 °C, showing the aromatic dipolar contacts for the methyls of Ile69(E18), Leu97(G5), and Val132(H18), at (A) pH 5.1 and (B) pH 8.5. NOESY cross peaks are labeled to demonstrate the following largely conserved dipolar contacts between: $C_\delta H_3$ of Ile69(E18) and the aromatic rings of Phes65(E14), 66(E15), and 128(H14), the methyls of the stationary Leu97(G5) to the Phe129(H15) ring, and the Val132-(H18) methyls to the rings of Phes 128(H14) and 133(H19), as well as the altered dipolar contacts between the Phe133(H19) ring and the stationary Leu97(G5) methyls and between the stationary Phe83(F4) ring and Val132(H18) methyls, that occur during the allosteric transition.

are carried out so as to ascertain the nature of similar structure changes that accompany the titration of the Bohr residue in cyanomet HbIII.

*Resonance Assignments.* The approaches to the assignments of the heme and heme cavity residues are the same as those described in detail earlier for the low-pH form for each cyanomet Hb (Zhang et al., 1996). Three helical fragments, Ile34(C4)-Lys37(C7), Phe65(E14)-Ile69(E18), and Phe83(F4)-Lys/Thr88(F9), characterized by standard backbone connectivities (Wüthrich, 1986) are identified as previously reported for the acidic protein. A fourth helical fragment of three residues earlier described for the acidic form (Zhang et al., 1996) was extended at both low pH and high pH to include the six residues Phe128-Phe129-X130-X131-Val132-Phe133, which reside on the H-helix portion H14-H19 (not shown; see Supporting Information). The Ile132(H18) in the HbIII structure was substituted by Val132-(H18) (Buse et al., 1979; Pfetschinger et al., 1980) in the low-pH or **t** state structure of HbIV and its side chain orientation set to be consistent with the observed NOE for one $C_\gamma H_3$ with the Phe83(F4) side chain (Figure 4A); the expected NOESY cross peaks of the other $C_\gamma H_3$ to Leu97-(G5), Val84(F5) (not shown), and Phe133(H19) ring (Figure 4A) were also observed at low pH. Other active site residues such as Phe38(CD1), parts of His58(E7), Lys61(E10), Ile62-(E11), parts of Arg90(FG3), Val92(FG5), parts of Leu97-(G5) and Phe100(G8), were located by the predicted heme contacts in the crystal at low pH (Steigemann & Weber, 1979), and the nature of the side chains was confirmed by the detection of the characteristic TOCSY cross peak topology [as reported previously at low pH (Zhang et al., 1996)]. Two additional relevant aromatic rings, one for Trp121(H7) and the other for Phe13(A12), were identified at low and high pH by the characteristic TOCSY connectivities and predicted NOESY cross peaks to the previously assigned Phe66(E15). The chemical shifts for the heme and the assigned residues at alkaline pH [$\delta_{DSS}$ (pH 8.5)], as well as the *change* in chemical shift upon converting the acidic form to the alkaline form,

$$\Delta\delta = \delta_{DSS}(\text{pH } 8.5) - \delta_{DSS}(\text{pH } 5.1) \qquad (2)$$

are listed in Tables 1 and 2 of Supporting Information.

*Environment of Titrating Residues.* The narrow signals in the aromatic spectral window, as candidates for His ring CH, were identified at both low and high pH by deconvolution, and the $C_\delta H$, $C_\epsilon H$ correlated by the observation of TOCSY peaks (not shown) between two pairs of such signals at long mixing times (King & Wright, 1982). Following the chemical shifts for these two His side chains as a function of pH led to significant chemical shift changes indicative of a pH titration of both residues with essentially indistinguishable p$K$ ~7.5 (not shown; see Supporting Information), which is the same as the p$K$ reflected by the heme hyperfine shifts (La Mar et al., 1978a). The two *Chironomus* Hbs each possess four His, of which two have been assigned previously to the hyperfine-shifted and relaxed proximal His87(F8) and distal His58(E7) (Peyton et al., 1991; Zhang et al., 1996), identifying the titrating residues as His94(G2) and His111(G19). The former His is found in a salt bridge with the terminal Met136(H22) on the proximal side of the heme, while the latter His is on the surface on the distal side in the crystal structures of HbIII (Steigemann & Weber, 1979). The assignment of the two titrating His rings was achieved by detecting NOEs for one His side chain to the assigned Leu97(G5), as expected for His94(G2). The remaining His111(G19) exhibits an NOE at pH 5.1 to a Tyr ring, as expected for the pair His111(G19) and Tyr107-(G15). The chemical shifts at alkaline pH and the pH-induced shift changes are listed in Table 2 of the Supporting Information.

A proton signal at low pH with a weakly temperature-dependent chemical shift near 2.5 ppm (indicative of a small but not negligible low-field dipolar shift), and with no detectable scalar correlation, exhibits NOESY cross peaks to the previously assigned His87(F8), Val92(FG5), and Leu97(G5) at low pH, as shown in the NOESY slices in Figure 5A. This uniquely identifies the $C_\epsilon H_3$ of Met136-(H22), as expected from the crystal structure (Steigemann & Weber, 1979). The pattern of NOESY-detected contacts between the heme and nearby residues, and among those residues determined previously for the low-pH form of cyanomet HbIV, is shown schematically in Figure 2. Completely conserved NOESY cross peak patterns and intensities are marked by solid lines.

*Influence of pH on the Heme.* The heme exhibits only very small changes in hyperfine shifts (shown in Table 1 of

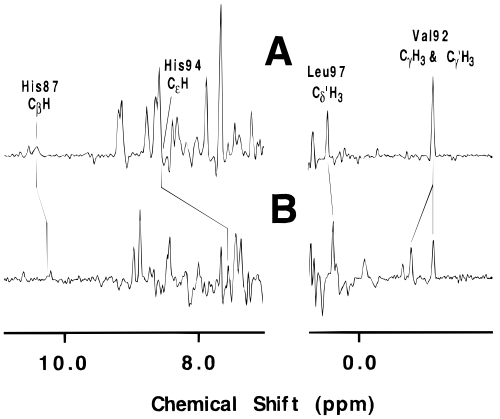


FIGURE 5: Slices of 500 MHz $^1$H NMR NOESY ($\tau_m$ = 110 ms) spectra for cyanomet HbIV in $^1H_2O$ at 20 °C, showing NOESY cross peaks to Met136(H22) $C_\epsilon H_3$ at (A) pH 5.1 and (B) pH 8.5. The peak intensities of Val92(FG5) $C_\gamma H_3$, $C_\gamma' H_3$, and Leu97(G5) $C_\delta' H_3$ are minimally altered, while the His87(F8) $C_\beta H$ peak intensity is significantly reduced at high pH and the cross peak to His94-(G2) $C_\epsilon H$ appears only at the alkaline pH. Other signals in the slices arise from protons nearly degenerate with Met136(H22) $C_\epsilon H_3$. The data show that the Met136(H22) side chain has oriented away from the axial His at alkaline pH. NOESY slice at the two pHs in each case were calibrated with constant amplitude for the diagonal of resolved proton signals whose $T_1$s are indistinguishable.

Supporting Information) for all signals[2] except the 4-vinyl group, which shows substantial shift changes as reported previously (La Mar et al., 1978a,b). The orientations of the 2-vinyl and the 6- and 7-propionate groups relative to the heme, as characterized by the NOESY cross peaks to the two adjacent heme protons, are unchanged with pH (not shown). The influence of pH on the NOESY cross peak pattern for 3-methyl is minimal (Figure 6A,B). The 4-vinyl group, however, exhibits significant changes not only in shift (Table 1, Supporting Information), but also in dipolar contacts (Figures 6C−H). The loss of the $4H_{\beta t}$ NOESY cross peak to the 5-methyl and the increase in NOESY cross peak intensity to Phe100(G8) at alkaline relative to acidic pH (Figure 6E, 6F) indicate that the mobility of the 4-vinyl group (detected even in the crystal structure) at acidic pH is restricted and constrained to adopt a more *cis* ($H_\beta$s closer to 3-methyl) than *trans* orientation at alkaline pH. Both the $H_\beta$s and $H_\alpha$ for the 4-vinyl group exhibit significantly altered contacts to Phe65(E14) and Ile69(E18) at pH 8.5 as well (Figures 6C−H).

*Residues Inconsequentially Perturbed by the* **t** → **r** *Transition.* For a large part, the assigned residues exhibit NOESY cross peak patterns (the involved protons and the relative intensities) to the heme and among each other, as well as paramagnetic induced relaxation, that are indistinguishable for the low- and high-pH forms for each of the three Hbs (Figure 2). The residues with highly conserved positions relative to the heme and to each other exhibited, for the most part, insignificantly altered (<0.1 ppm) chemical shifts (with some exceptions; see below). The proximal residues which exhibit unaltered spatial contacts with minimal shift changes are the backbone and side chains for the F-helix residues Phe83(F4) to His87(F8) [however, see

[2] The pattern of alternating upfield and downfield shifts for the four methyl and four *meso*-Hs are consistent with a rotation of ~1° of the rhombic *magnetic axes* (Lee et al., 1994). This very minor accommodation of the heme may result from changed van der Waals contacts between pyrrole B and E-helix side chains (see text).

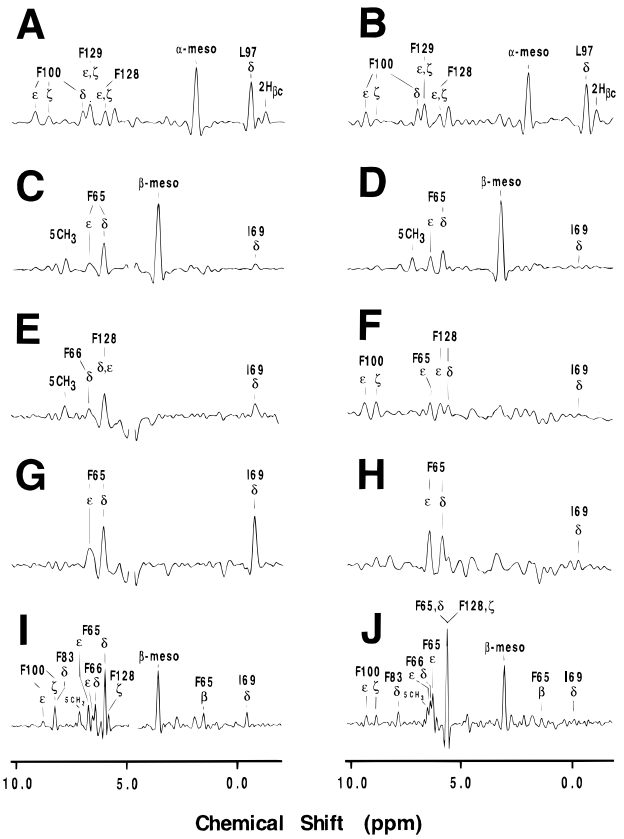


FIGURE 6: Slices of the $^1$H NMR NOESY ($\tau_m$ = 50 ms) spectra of cyanomet HbIV in $^1H_2O$ at 30 °C for the resolved signals of the heme pyrrole B substituents at pH 5.1 (A, C, E, G) and pH 8.5 (B, D, F, H) through the diagonals of (A, B) 3-$CH_3$ with largely conserved contacts to the rings of Phes100(G8), 128(H14), and 129-(H15) and the methyl of Leu97(G5); (C, D) $4H_\alpha$ showing altered Phe65(E14) ring contacts at alkaline pH; (E, F) $4H_{\beta t}$ illustrating loss of 5-$CH_3$ cross peak, increased intensity cross peak to stationary Phe100(G8) ring and altered contact to the ring of Phe65(E14) and Phe66(E15) at alkaline pH; (G, H) and $4H_{\beta c}$ demonstrating loss of Ile69(E18) $C_\delta H_3$ contact and altered contact to the Phe65(E14) ring upon converting to the high-pH form. NOESY slice through the 4-$CH_3$ of cyanomet HbIV* (HbIV reconstituted with protoheme III with $R_3$ = vinyl and $R_4$ = methyl in Figure 2) in $^2H_2O$ at 30 °C at (I) pH 5.1, and (J) pH 8.5 showing stronger cross peaks to the ring of Phe65(E14) and loss of Ile69(E18) $C_\delta H_3$ NOE at alkaline pH. NOESY slice at the two pHs in each case were calibrated with constant amplitude for the diagonal of resolved proton signals whose $T_1$s are indistinguishable.

results for Phe83(F4)/Val84(F5) below]. In particular, the detailed NOESY cross peak pattern to both heme and the F-helix backbone is maintained for the side chain of Phe83-(F4). The unaltered dipolar contacts between Val92(FG5) and both His87(F8) and the pyrrole A substituents, Arg90-(FG3) and both His87(F8) and 8-methyl, as well as between the proximal Leu97(G5) and the heme, axial His87(F8) and Val92(FG5), confirm highly conserved orientations with pH for the residues on the F helix, G helix and FG corner relative to each other and the heme. The distal residues (shown as squares in Figure 2), Phe38(CD1), His58(E7), Lys61(E10), $C_\alpha H$ of Ile62(E11), Ile34(C4), and Phe100(G8), exhibit small shift changes (see below) but completely unaltered paramagnetic relaxivities and NOESY cross peak patterns to the heme and among each other, indicating that the allosteric transition does not significantly perturb any portion of the distal pocket. In our subsequent analysis of pH-perturbed region of the heme cavity, we make the simplifying assumption that the side chains of the F-helix [Phe83(F4), Val84-

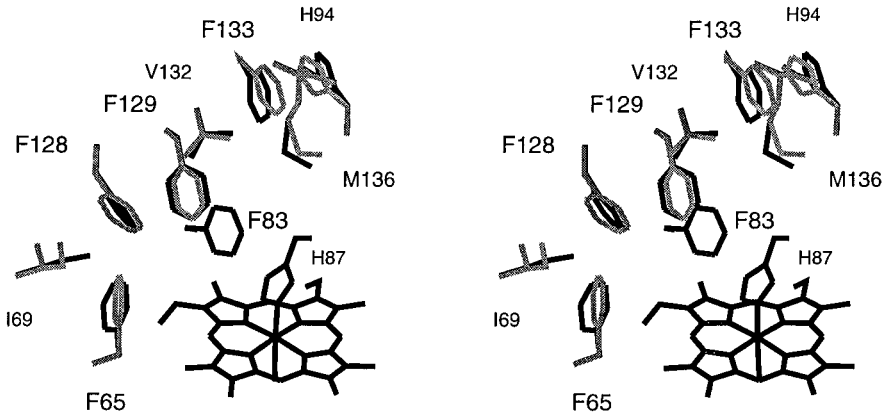


FIGURE 7: Stereoviews of heme and amino acid side chains of residues involved in the allosteric transition in *CTT* cyanomet HbIV [Phe65(E14), Ile69(E18), His94(G2), Phe128(H14), Phe129(H15), Val132(H128), Phe133(H19), and Met136(H22)], as well as two stationary residues, Phe83(F4) and His87(F8). The side chain orientations for the low-affinity, low-pH, or **t** state are shown in dark lines as defined by the cyanomet HbIII crystal structure and confirmed in solution for both cyanomet HbIII and HbIV (Zhang et al., 1996). The altered orientations, as deduced from NMR data for the high-affinity, high-pH form (or **r** state) are shown in shaded lines.

(F4), His87(F8)], FG corner [Lys90(FG3), Val92(FG5)], and G-helix [Leu97(G5), Phe100(G8)], and all distal residues except Phe66(E15) (see below) are completely conserved in the allosteric transition, and use these conserved proximal residues to define the contacts that are significantly altered at pH 8.5 relative to pH 5.1.

*Heme Pocket Regions Perturbed by the* **t** → **r** *Transition.* Two regions of the heme cavity, both primarily on the proximal side of the heme, exhibit significant shift changes and altered NOESY cross peak patterns at pH 8.5 relative to those observed at pH 5.1. One region is near the junction of pyrroles A and B (top of Figure 2), with relevant NOESY slices shown in Figure 5. When the pH is increased, the NOESY cross peak between Met136(H22) $C_\epsilon H_3$ and the conserved His87(F8) $C_\beta H$ is significantly reduced in intensity, and there is observed at high pH a new NOESY cross peak from Met136(H22) $C_\epsilon H_3$ to the His94(G2) ring. The appearance at alkaline pH of a NOESY cross peak between the Phe133(H19) and His94(G2) side chains (not shown) is consistent with small rotations of both side chains which stack the Phe and neutral His rings. The small rotation of the Phe133(H19) side chain also results in reduced NOESY cross peak intensity between Phe133(H19) $C_\epsilon Hs$ and the methyls of the stationary Leu97(G5) (Figures 4A and 5B). The observed pH-induced structural changes are consistent with the rupture at high pH (**r** state) of the salt bridge between the carboxylate of the terminal Met136(H22) and the imidazolium side chain of His94(G2), with the result that the Met136(H22) side chain moves away from the axial His87(F8) and toward His94(G2).

Val132(H18) in the HbIII crystal structure was replaced by Ile132 to correspond to the HbIV structure and its orientation at pH 5.1 set by the observed NOESY peak for one methyl to the ring of Phe83(F4) (Figure 4A), and the other to Leu G5, Val84(F5) (not shown) and Phe133(H19) (Figure 4A). Upon converting to high pH, Val132(H18) $\chi_1$ changes by ~20° to place both methyls in close contact with the stationary Phe83(F4) side chain (Figure 4B). A NOESY cross peak between Val132(H18) $C_\beta H$ and Phe129(H15) $C_\delta Hs$ at alkaline pH (not shown), which cannot be accounted for by the small rotation of the former residue, indicates that the Phe129(H15) ring also rotates ($\chi_2$) by ~20°, as evidenced by the changed NOEs to Phe128(H14) ring protons (not shown), and largely conserved NOESY cross peaks for $C_\xi H$ and $C_\epsilon Hs$ to 3-$CH_3$ (Figure 6A,B) and Phe100(G8) (not shown). The structure of HbIV with the Ile(H18) → Val substitution relative to HbIII *has the space to accommodate this Phe129(H15) ring reorientation* (see below). An increase in the NOESY cross peak intensity between the side chain of Phe129(H15) and Phe128(H14) is due, in part, to the above described rotation of the Phe129(H15) ring. This rotation of the Phe129(H15) ring, however, cannot by itself account for the ~0.4 ppm upfield shift at alkaline pH (Table 2 of Supporting Information) of the averaged $C_\delta H$ peak of Phe128(H14), but is consistent with the Phe128(H14) ring rotating ($\chi_2$) by ~20° toward a more perpendicular orientation to the Phe129(H15) ring. The proposed altered orientations of these residues are illustrated in shaded lines in the stereoview in Figure 7.

The other region of the heme pocket where significant perturbations of both NOESY cross peak pattern and shifts are observed is found in the contacts between pyrroles B and C and the E-helix (left side of Figure 2) and involves residues Phe65(E14), Phe66(E15), Ile69(E18), with relevant NOESY data shown in Figure 6. Conversion to the high-pH form leads to altered NOEs between 5-$CH_3$ and Phe65(E14) $C_\beta Hs$ (not shown), indicating a change in $\chi_1$ to place the Phe65(E14) ring close to pyrrole B (*i.e.*, the 4-vinyl group), as well as strongly altered contacts between the 4-vinyl group and the side chains of Phe65(E14) and Ile69(H18) (Figures 6C−H); increased intensity NOESY cross peak for the Phe65(E14) ring to the Phe66(E15) peptide NH (not shown; see Supporting Information) also supports a Phe65(E14) ring reorientation toward the 4-vinyl group. The fact that *both the 4-vinyl group (see above) and the Phe65-(E14) ring* rotate in the allosteric transition obscures the nature of the latter reorientation in cyanomet HbIV. However, in cyanomet HbIV* the crucial position is occupied by the 4-methyl group, whose NOESY slices clearly show increased cross peak intensity to the Phe65(E14) ring and the loss of the cross peak to Ile69(E18) at alkaline (Figure 6J) relative to acidic pH (Figure 6I) (as well as the conserved 4-$CH_3$ NOEs to the Phe83(F4) and Phe100(G8) rings). Lastly, the NOESY cross peak pattern between the side chains of Phe65(E14) and Ile69(E18), both of which rotate, is qualitatively retained (Figure 4). The change in NOESY cross peak pattern near the junction of pyrroles B and C is consistent with a rotation of the Phe65(E14) side chain ($\chi_1$)

by ~20° to take the ring closer to the 4-vinyl group (or, in cyanometHbIV*, the 4-methyl).

The rotation of the Ile69(E18) side chain is such to vacate space for the position of Phe65(E14) in the alkaline form. The two portions of the proximal side of the heme strongly perturbed by the allosteric transition are clearly linked by the reorientation of the Phe128(H14) ring. The shift changes for F-helix residues with *essentially unperturbed* NOESY pattern, and hence conserved structure in the low- to high-pH forms, are readily interpreted on the basis of changed contacts to residues whose orientation depends on pH [*i.e.*, loss of Met136(H22) $S_\delta$ contact to the Val84(F5) backbone and ring current effects of the Phe65(E14) ring on Phe83(F4) $C_\beta$Hs at alkaline pH]. The 4-vinyl shift changes reflect accommodation of its restricted mobility (La Mar et al., 1978b) and the increased ring currents of Phe65(E14) at alkaline pH. The changes in side chain orientations with pH are illustrated in Figure 7.

*Magnetic Axes Determination.* The magnetic axes for cyanomet HbIV at alkaline pH were determined using the same proximal side F-helix and FG corner residues used as input at acidic pH (Zhang et al., 1996). The resulting magnetic axes at high pH were found essentially indistinguishable from those reported earlier at low pH (not shown; see Supporting Information). This conclusion could have been anticipated on the basis of minimal chemical shift changes for these residues. The small changes in shifts for distal residues (~2.5% change in dipolar shifts), in spite of the conserved magnetic axes, suggests a small but systematic perturbation of the distal relative to the proximal side. Attempts to correlate the distal side chain shifts with changed tilt magnitude with conserved direction of tilt, or changed direction for conserved tilt magnitude, failed to account for the shifts. However, a ~0.2 Å translation of the distal residues over the heme toward the $\gamma$-*meso*-H along the $\alpha,\gamma$-*meso* vector (or, the reverse translation of the heme) quantitatively accounts for the shift change for distal residues (not shown; see Supporting Information).

The three *proximal residue side chains* in contact with heme and/or axial His with significant dipolar shifts, and whose orientation changes significantly in the allosteric transition, are Phe65(E14), Ile69(E18), and Met136(H22). While their dipolar shifts were well predicted in the low-pH or **t** state (Zhang et al., 1996), a similarly quantitative assessment at high pH is not practical, since the altered orientation for these residues are as much influenced by altered diamagnetic ring current effects of the heme and other Phe side chains as from altered dipolar shifts. For the Met136(H22) $C_\epsilon H_3$ and Ile69(E18) $C_\delta H_3$, the small upfield and large low-field shift biases, respectively, at high relative to low pH are completely consistent with the predicted decreased downfield and upfield dipolar shifts, respectively, at high pH. In the case of the Phe65(E14) ring, the proposed ~20° change in $\chi_1$ leads to only a ~0.2 upfield bias for $C_\zeta$H, as compared to an observed $\Delta\delta = 0.6$ ppm. The observed $\Delta\delta$ 0.6 ppm would require a change by 45° rather than just 20° (not shown; see Supporting Information).

*pH Influence on Cyanomet HbIII.* The assignment of the majority of key residues in cyanomet HbIII at alkaline pH was similarly carried out, and the chemical shifts and NOESY cross peak patterns (not shown) at pH 5.1 and 8.5 were compared. The observed pH influences on chemical shifts are listed in Tables 1 and 2 of the Supporting Information. The patterns of shift changes for relevant residues and the heme due to the His94(G2) titration are very similar to those described above for cyanomet HbIV, except that the *changes for the heme and for the three key residues, Met136(H22), Phe65(E14), and Ile69(E18), in cyanomet HbIII are much smaller than those observed for cyanomet HbIV*. The lower spectral sensitivity for cyanomet HbIII relative to cyanomet HbIV, due to the less favorable ratio of heme orientational isomers and presence of a silent mutation, did not allow the definitive identification of changes in NOESY cross peak pattern in the alkaline relative to acidic pH. It is noted that both His94(G2) and His111(G19) titrate with the same p*K* as evidenced by the ring chemical shift changes that are the same as observed in cyanomet HbIV. The smaller Bohr effect amplitude of HbIII than that of HbIV (Sick & Gersonde, 1969, 1974; Gersonde et al., 1972, 1976) appears to be reflected by the smaller spectral influences of pH for cyanomet HbIII.

## DISCUSSION

*Bohr Proton Site*. The chemical shift changes with pH for His94(G2) and His111(G19) in cyanomet HbIV show that both side chains titrate with essentially indistinguishable p*K*s of ~7.5. However, only one of these residues is linked to the Bohr effect since both the ligand affinity and the chemical shift changes in the heme vicinity in all oxidation/ligation states follow the Henderson−Hasselbalch equation for the titration of a single proton (Sick & Gersonde, 1969; Gersonde et al., 1972; La Mar et al., 1978a). The titration of His111(G19) leads to the loss of the NOESY cross peak to Tyr107(G15), but otherwise no significant NOESY peak patterns were observed in the vicinity of these residues. The titration of His94(G2), in contrast, is linked directly to significant structural changes involving Met136(H22) and adjacent residues, and hence is identified as the Bohr proton site in both HbIV and HbIII. The titration of His94(G2), moreover, can be traced directly to the complete range of structural changes observed in the allosteric transition. This assignment of His94(G2) as the origin of the Bohr proton had been proposed earlier solely on the basis on its position relative to Met136(H22) in the crystal structure of HbIII (Sick et al., 1972; Krümpelmann et al., 1980a).

*Mechanism of the Bohr Effect in Cyanomet HbIV*. The $^1$H NMR data show that the conversion to pH 8.5 *leaves the distal pocket structure of cyanomet HbIV largely unperturbed relative to that in the low-pH or* **t** *structure*. This lack of significant distal perturbations is underscored by the insignificant change (0.3%) in the large $^{15}$N hyperfine shift (~600 ppm) for the ligated cyanide (Sick et al., 1980). In fact, the significant structural changes in the heme pocket are in the region near the axial His and titrating His94(G2) [Met136(H22), Phe133(H19), Val132(H18), Phe129(H15)] and the pyrrole B/C junction [Phe65(E14), Ile69(E18)), as well as the link between these two regions (Phe128(H14)], and lie on the *proximal* side of the heme (Figures 2 and 7). These proximal perturbations are readily detected and can be quantitated to some degree because key proton signals are either resolved (4-vinyl, 3-methyl) or exhibit sufficient hyperfine shift [Met136(H22), His87(F8), Phe65(E14), Ile69(E18)] so as to allow the resolution of the cross peak of interest at some accessible temperature. The NOESY contacts to the resolved 8-methyl, 7-propionate $H_\alpha$, and Phe38(CD1) $C_\zeta$H signal similarly allow the conclusion that

the heme contacts are unperturbed in the pH 5.1−8.5 transition. The remaining contacts to the heme occur solely within the diamagnetic envelope, require several temperatures to resolve the multiple degeneracies, and hence preclude quantitative comparison of NOESY cross peak intensity at the two pH values. However, the inconsequential chemical shift changes and the few cross peaks that are resolved confirm conserved environments for pyrroles A and C [except for the Phe65(E14) contact; see below].

The residues whose side chains exhibit significant changes in orientation with pH are part of an extended hydrophobic and tightly packed region of the protein that constitutes the heme contacts with the H- and E-helices as shown in Figure 7. The pH-induced structural changes in this region for cyanomet HbIV allow the proposal of a mechanism for the Bohr effect that controls the ligand affinity via interactions that modulate the spacing between the F-helix and heme. Thus the structural changes described in Figure 7 can be considered to result from the following chain of events starting with the low-pH form (Zhang et al., 1996), with relevant van der Waals contacts shown in Figure 8A. The loss of the Bohr proton cleaves the salt bridge between His94(G2) and the Met136(H22) carboxy terminus, leads to the expulsion of the Met136(H22) terminus from its place adjacent to the axial His87(F8), and leads to rotation of the His94(G2) side chain and that of Phe133(H19) to allow for effective stacking of the two rings. The observed small rotation of Val132(H18) maintains the van der Waals contact to the rotated Phe133(H19) ring. The rotation of Phe133-(H19) breaks a van der Waals contact to the Phe129(H15) ring which, together with a space near Val132(H18) (see below), leads to its ring rotating by ∼20° from that at low pH. The rotation of Phe129(H15), in order to maintain close van der Waals contacts with its neighbors, leads to the described rotation of Phe128(H14). The rotation of this latter residue, however, results in a significant steric interaction with the low-pH orientation of Ile69(E18) (as shown in Figure 8B), whose subsequent reorientation at alkaline pH breaks the van der Waals contact to the heme. The reorientation of Ile69(E18) creates a hydrophobic pocket near pyrrole B which is filled by the subsequent rotation of Phe65-(E14), as shown in Figure 8C. Hence the structural transition can be described as a series of side chain rotations, initiated by the rotation of Phe133(H19), that maintain strong Van der Waals contacts among the residues in this hydrophobic region of the protein.

The position of the Met136(H22) side chain terminus and the Phe65(E14) ring at low pH in the **t** state can be viewed as providing spacers between the F-helix and heme and between the E- and F-helix backbones, respectively, as shown in Figure 9A, that impede the movement of the iron into the heme plane and hence result in the low-affinity or **t** state. With the Bohr site deprotonation and the cascade of side chain reorientations that result in the expulsion of the Met136(H22) and rotation of the Phe65(E14) side chain, these impediments are removed in the high-affinity or **r** state, as shown in Figure 9B.

*Structure of the* **r** *State in HbIV*. There is a question, however, whether the high-pH form [even if the deprotonation of His94(G2) is completed (99%) at pH 9.5] of cyanomet HbIV represents solely a new structure or simply a shift in the equilibrium in eq 1 toward significant population of the **r** state. In all cases the molecular model allows larger

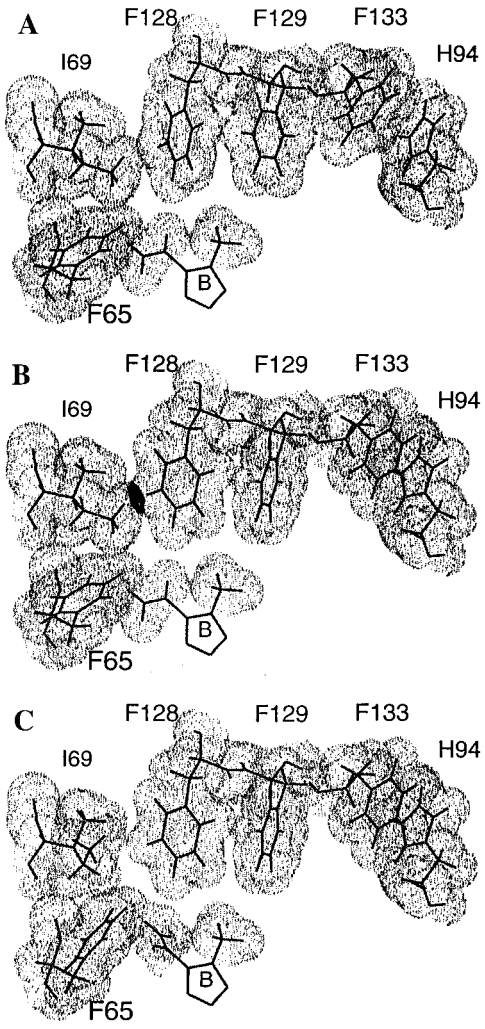


FIGURE 8: Van der Waals surfaces (shaded areas) of key residues in transmitting the Bohr effect from His94(G2) to side chains of the H and E helices in HbIV. (A) pH 5.1 (**t** state), as found in the crystal of cyanomet HbIII and confirmed in solution for both HbIII and HbIV (Zhang et al., 1996); (B) after rotations of Phe133(H19), Phe128(H14), Phe129(H15), and His94(G2), which create a steric overlap (solid area) between the Phe128(H14) ring and the Ile69-(E18) side chain; and (C), after reorientation of Ile69(E18) to eliminate the steric repulsion with the reoriented Phe128(H14), followed by rotation of the ring of Phe65(E14) into the space vacated by Ile69(E18).

rotation of residues than those crudely estimated to qualitatively account for observed NOESY intensity changes. However, similar effects could arise from a *partial population of a structure with much larger rotation of the perturbed residues*. In the absence of a more definitive model for the **r** state, the present NMR data do not allow a differentiation between the two alternatives. However, because of the observations for cyanomet HbIII (see below), we favor a partial but significant, as opposed to complete, population of the **r** state for cyanomet HbIV when His94(G2) is deprotonated. The position of the equilibrium in eq 1, upon deprotonation of the Bohr site, would depend on ligand.

*Structural Origin of Differential Bohr Effects in HbIII and HbIV*. The amplitudes of the Bohr effect for both $O_2$ and CO binding is larger for HbIV than HbIII (Sick & Gersonde, 1969, 1974; Gersonde et al., 1972, 1976). The above proposed mechanism of the Bohr effect in cyanomet HbIV that leads to only partial population of the **r** state at high-pH lends itself to a structural hypothesis for the much lower

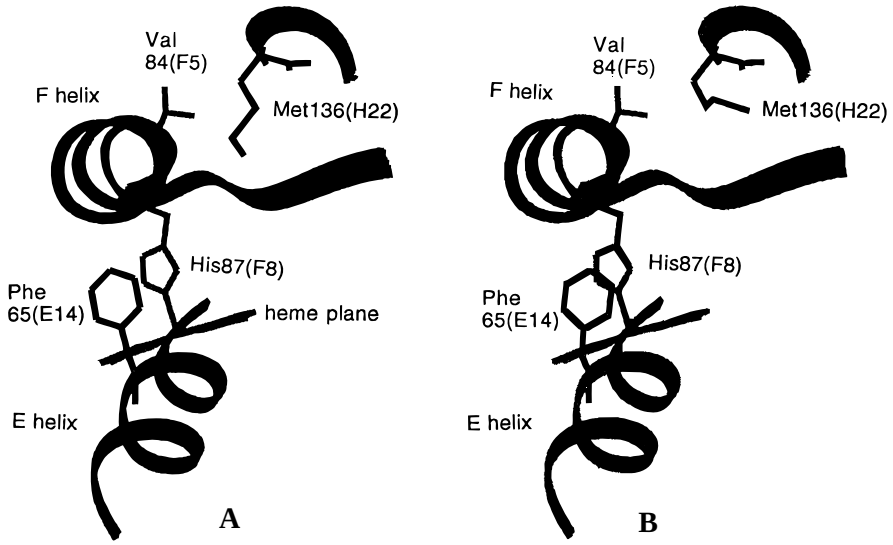


FIGURE 9: Schematic representation of (A) the roles of Phe65(E14) and Met136(H22) side chains as spacers between the F-helix and heme in the low-pH, low-affinity (**t**) state which impede the movement of the heme iron into the heme plane, and (B) the removal of these impediments by the reorientation of Phe65(E14) and Met136(H22) at the high-pH, high-affinity (**r**) state.

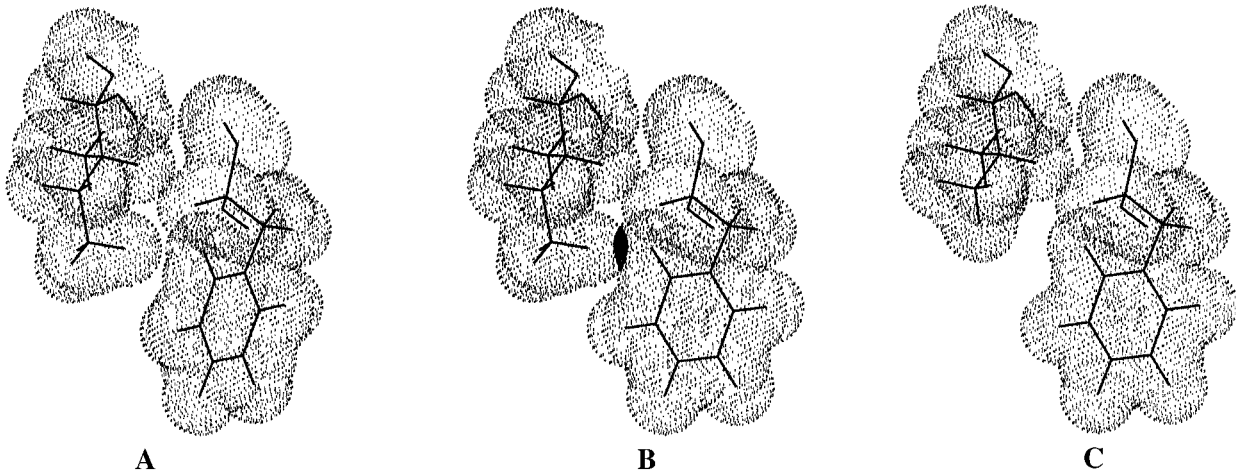


FIGURE 10: Influence of residue 132(H18) on the transmission of the Bohr effect in *CTT* Hb (A) the van der Waals surfaces (shaded areas) for the orientations of Ile132(H18) and Phe129(H15) in the low-pH or low-affinity (**t**) state, as found in the crystal structure of cyanomet HbIII [and proposed to exist in the same form, except for the deleted $C_\delta H_3$ and minor reorientation of residue 132(H18) in cyanomet HbIV (Zhang et al., 1996)]. (B) The ~20° rotation of the Phe129(H15) ring induced by the stacking of Phe133(H19) and His94(G2) leads to steric interference of ~0.5 Å van der Waals overlap (solid area) with the $C_\delta H_3$ of Ile132(H18) in alkaline cyanomet HbIII, and (C), the high-pH orientation of the same residues in cyanomet HbIV where the deletion of $C_\delta H_3$ in Ile132(H18)→Val eliminates the steric barrier.

Bohr effect amplitude in HbIII than HbIV and lends further support that the Bohr proton modulates the relative stability of the **t** and **r** states such that the **r** state is only fractionally populated at high pH. Since the low-pH or **t** structures of cyanomet HbIII and HbIV have been shown to be very similar (Zhang et al., 1996), the similar changes in shift patterns with pH, but with significantly reduced magnitude in HbIII, suggest that the **r** state in HbIII (in the cyanomet state) *is less stable* than HbIV relative to a more or less common **t** ground state. It is reasonable to assume that a similar situation pertains to the HbCO and $HbO_2$ complexes, and hence the present model can account for the HbIV, HbIII differential Bohr effects (Sick & Gersonde, 1969, 1974; Gersonde et al., 1972, 1976). The only sequence difference between HbIII and HbIV for a nonsurface residue is Ile-(HbIII) *vs* Val(HbIV) at position 132(H18). The rotation of Phe133(H19) to stack with the neutral Bohr residue His94-(G2) allows the rotation of Phe129(H15) in HbIV *because of an interior vacancy if position 132(H18) is occupied by a Val* (as in HbIV). In HbIII, Ile132(H18) is tightly packed and the movement of Phe133(H19) would be insufficient by itself to allow the rotation of Phe129(H15). Hence, the **r** state of HbIII would be less stable relative to **t** state, and hence much less populated, than for HbIV. Although variable surface residues likely also play some role in modulating the relative stability of the **r** state in the two Hbs, the internal substitution appears as the major determinant of the amplitude of the Bohr effect in the *Chironomus* Hb. The present analysis leads to the prediction that mutation of Ile132(H18)→Val in HbIII will result in a dramatic increase in its Bohr effect amplitude.

## CONCLUSIONS

The Bohr effect in the monomeric HbIII and HbIV from *C. thummi thummi* is shown to result from the deprotonation of His94(G2), which breaks the salt bridge to the carboxy terminus Met136(H22), results in a rotation of Phe133(H19) which initiates a series of reorientations of primarily side chains on the H- and E-helices that leads ultimately to the rotation of the Phe65(E14) ring in contact with the heme.

The expulsions of the Met136(H22) side chain terminus between the heme and F-helix backbone and the ring of Phe65(E14) from between the E- and F-helices during the allosteric transition, relaxes the constraints on the movement of the F-helix toward the heme that is necessary for effective ligation.

## ACKNOWLEDGMENT

The authors are indebted to Dr. J. S. de Ropp for experimental assistance.

## SUPPORTING INFORMATION AVAILABLE

Two tables (chemical shifts for heme and heme pocket residues and the influence of pH on chemical shifts for cyanomet-HbIII, -metHbIV, and -metHbIV*) and six figures [H-helix sequential assignment; pH titration of His ring signals; NOESY slices at two pHs through $C_\delta H$ of Phe65-(E14); plot of observed *vs* predicted dipolar shifts on determined magnetic axes; plot of observed and predicted dipolar shifts from heme translation; and plot of effect of $\chi_1$ bond rotation of Phe65(E14) on the $C_\xi H$ dipolar shift] (10 pages). Ordering information is given on any current masthead page.

## REFERENCES

Bax, A. (1981) *Two-Dimensional Nuclear Magnetic Resonance in Liquids*, Delft University Press, Delft, The Netherlands.
Bax, A., & Davis, D. G. (1985) *J. Magn. Reson. 65*, 355−360.
Bertini, I., & Luchinat, C. (1986) *NMR of Paramagnetic Molecules in Biological Systems*, Benjamin Cummings, Menlo Park, CA, pp 47−83.
Braunitzer, G., & Braun, V. (1965) *Z. Physiol. 340*, 88−91.
Braunschweiler, L., & Ernst, R. R. (1983) *J. Magn. Reson. 53*, 521−528.
Buse, G., Steffens, G. J., Braunitzer, G., & Steer, W. (1979) *Hoppe-Seyler's Z. Physiol. Chem. 360*, 89−97.
Cross, K. J., & Wright, P. E. (1985) *J. Magn. Reson. 64*, 220−231.
Dickerson, R. E., & Geis, I. (1983) *Hemoglobins: Structure, Function, Evolution, Pathology*, Benjamin-Cummings, Menlo Park, CA.
Emerson, S. D., & La Mar, G. N. (1990) *Biochemistry 29*, 1556−1566.
Gersonde, K., Sick, H., Wollmer, A., & Buse, G. (1972) *Eur. J. Biochem. 25*, 181−189.
Gersonde, K., Noll, L., Gaud, H. T., & Gill, S. J. (1976) *Eur. J. Biochem. 62*, 577−582.
Gersonde, K., Sick, H., Overkamp, M., Smith, K. M., & Parish, D. W. (1986a) *Eur. J. Biochem. 157*, 393−404.
Gersonde, K., Kerr, E., Yu, N.-T., Parish, D. W., & Smith, K. M. (1986b) *J. Biol. Chem. 261*, 8678−8685.
Hartmann, H., Steigemann, W., Reuscher, H., & Parak, F. (1987) *Eur. Biophys. J. 14*, 337−348.
Huber, R., Epp, O., Steigemann, W., & Fromanek, H. (1971) *Eur. J. Biochem. 19*, 142−150.
Kao, W.-Y., Trewitt, P. M., & Bergstrom, G. (1994) *J. Mol. Evol.* 38, 241−245.
King, G., & Wright, P. E. (1982) *Biochem. Biophys. Res. Commun. 106*, 559−565.
Krümpelmann, D., Ribbing, W., & Rüterjans, H. (1980) *Eur. J. Biochem. 108*, 103−109.
La Mar, G. N., & de Ropp, J. S. (1993) in *Biological Magnetic Resonance* (Berliner, L. J., & Reuben, J., Eds. Vol. 18, pp 1−78, Plenum Press, New York.
La Mar, G. N., Overkamp, M., Sick, H., & Gersonde, K. (1978a) *Biochemistry, 17*, 352−361.
La Mar, G. N., Viscio, D. B., Gersonde, K., & Sick, H. (1978b) *Biochemistry 17*, 362−367.
La Mar, G. N., Smith, K. M., Gersonde, K., Sick, H., & Overkamp, M. (1980) *J. Biol. Chem. 255*, 66−70.
La Mar, G. N., Anderson, R. R., Chacko, V. P., & Gersonde, K. (1983) *Eur. J. Biochem. 136*, 161−166.
Lee, K.-B., La Mar, G. N., Mansfield, K. E., Smith, K. M., Pochapsky, T. C., & Sligar, S. G. (1993) *Biochim. Biophys. Acta A1202*, 189−199
Perutz, M. F., Fermi, G., Luisi, B., Shaanan, B., & Liddington, R. C. (1987) *Acc. Chem. Res. 20*, 309−321.
Peyton, D. H., La Mar, G. N., & Gersonde, K. (1988) *Biochim. Biophys. Acta 954*, 82−94.
Peyton, D. H., La Mar, G. N., Ramaprasad, S., Unger, S., Sankar, S., & Gersonde, K. (1991) *J. Mol. Biol. 221*, 1015−1026.
Pfletschinger, J., Plagens, H., & Braunitzer, G. (1980) *Z. Naturforsch. 35c*, 840−843.
Qin, J., & La Mar, G. N. (1992) *J. Biomol. NMR 2*, 597−618.
Qin, J., La Mar, G. N., Ascoli, F., & Brunori, M. (1993) *J. Mol. Biol. 231*, 1009−1023.
Rajarathnam, K., La Mar, G. N., Chiu, M. L., & Sligar, S. G. (1992) *J. Am. Chem. Soc. 114*, 9048−9058.
Rajarathnam, K., Qin, J., La Mar, G. N., Chiu, M. L., & Sligar, S. G. (1993) *Biochemistry 32*, 5670−5680.
Ribbing, W., & Rüterjans, H. (1980) *Eur. J. Biochem. 108*, 89−102.
Ruf, H., Altemüller, A. G., & Gersonde, K. (1994) *Methods Enzymol. 231*, 95−111.
Sick, H., & Gersonde, K. (1969) *Eur. J. Biochem. 7*, 273−297.
Sick, H., & Gersonde, K. (1974) *Eur. J. Biochem. 45*, 313−320.
Sick, H., Gersonde, K., Thompson, J. C., Maurer, W., Haar, W., & Rüterjans, H. (1972) *Eur. J. Biochem. 29*, 217−223.
Sick, H., Gersonde, K., & La Mar, G. N. (1980) *Hoppe-Seyler's Z. Physiol. Chem. 361*, 333−334.
States, D. J., Haberkorn, R. A., & Reuben, D. J. (1982) *J. Magn. Reson. 48*, 286−292.
Steffens, G., Buse, G., & Wollmer, A. (1977) *Eur. J. Biochem 72*, 201−206.
Steigemann, W., & Weber, E. (1979) *J. Mol. Biol. 127*, 309−338.
Wishart, D. S., Sykes, B. D., & Richards, F. M. (1991) *J. Mol. Biol. 222*, 311−333.
Wüthrich, K. (1986) *NMR of Proteins and Nucleic Acids*, Wiley, New York.
Zhang, W., La Mar, G., & Gersonde, K. (1996) *Eur. J. Biochem. 237*, 841−853.

BI9626463